Available online at www.sciencedirect.com
SCIENCE DIRECT
Journal of Photochemistry and Photobiology A: Chemistry 174 (2005) 82–87
Journal of Photochemistry and Photobiology A:Chemistry
www.elsevier.com/locate/jphotochem

The dc thermal plasma synthesis of ZnO nanoparticles for visible-light photocatalyst

Hsiu-Fen Lin *, Shih-Chieh Liao, Sung-Wei Hung

Materials Research Laboratories, Industrial Technology Research Institute, Hsinchu 31040, Taiwan, ROC

Received 1 October 2004; received in revised form 6 January 2005; accepted 28 February 2005
Available online 12 May 2005

Abstract

It is known that ZnO is an n-typed semiconductor with band-gap energy of ∼3.2 eV and thus only absorbs UV light with the wavelength ≤385 nm. However, as far as photocatalytic efficiency and practical applications are concerned, it is desirable that ZnO absorbs not only UV but also visible light. In the present study, a novel dc thermal plasma reactor was used to synthesize ZnO nano-particles. We found that the kind of plasma affects the nanoparticle morphology and N_2 plasma favors formation of the spherical nanoparticles. Visible light absorption of the ZnO nano-particles was achieved by doping up to a few thousands ppm of nitrogen into the material. The effect of doping concentration and particle morphology on photocatalytic characteristics of the ZnO nanoparticles will be described.

Keywords: Nano particle; dc plasma; Visible-light photocatalyst

1. Introduction

Zinc oxide (ZnO) nanoparticles have recently received much attention due to a variety of applications such as UV absorption, NO_X decomposition, deodorization, and anti-bacterial treatment [1–3]. Various techniques have been used to synthesize ZnO nanoparticles and can be categorized into either chemical or physical methods [4]. The former are, for example, thermal hydrolysis technique [5], hydrothermal processing [6], and sol–gel method [7–9] while the latter are vapor condensation method [10], spray pyrolysis [11–13], and thermochemical/flame decomposition of metal-organic precursors [14,15]. It is known that ZnO is an *n*-type semiconductor with band-gap energy of 3.2 eV and thus can absorb UV light with the wavelength equal or less than 385 nm. However, for higher photocatalytic efficiency and many practical applications, it is desirable that photocatalyst such as ZnO should absorb not only UV but also visible light due to the fact that visible light accounts for 45% of energy in the solar radiation while UV light less than 10%. In order to absorb visible light, band gap of ZnO has to be narrowed or split into several sub-gaps, which can be achieved by implanting transitional metal ions, e.g. V, Cr or Fe [16–19], or by doping N [20–23].

In the present study, we used a novel dc thermal plasma technology to synthesize N-doped ZnO nanoparticles. The effect of nitrogen doping and particle morphology on photocatalytic characteristics of the ZnO nanoparticles will be described.

2. Experimental

2.1. Synthesis of ZnO nanoparticles

In the present study, a novel dc plasma reactor (Fig. 1) operated at 70 kW and atmospheric pressure was used to synthesize ZnO nanoparticles. Commercial zinc powder (Alfa Aesar) with an average particle size of 10 μm and containing impurities of Cr Fe and Pb less than 50 ppm were used as the raw material. The Zn powders were fed into plasma flame through carrier gas and subsequently underwent vaporization, oxidation and quench processes. Dop-

* Corresponding author. Tel.: +886 3 5917934; fax: +886 3 5820039.
E-mail address: linshufeng@itri.org.tw (H.-F. Lin).

1010-6030/$ – see front matter © 2005 Elsevier B.V. All rights reserved.
doi:10.1016/j.jphotochem.2005.02.015

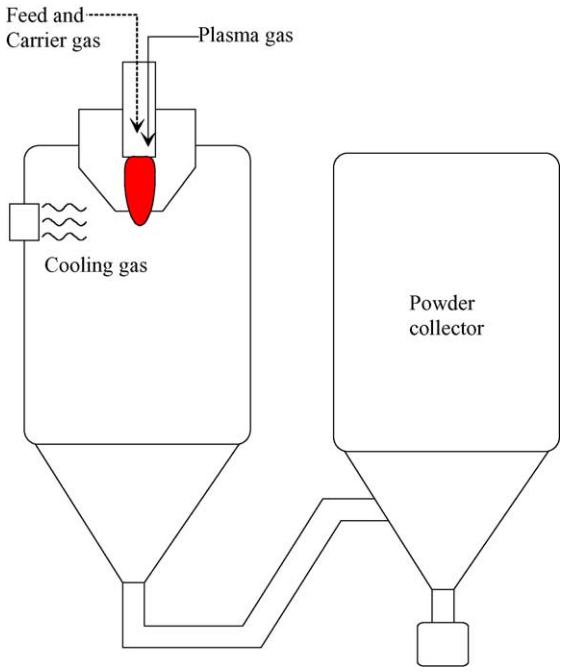

Fig. 1. Schematic of the dc plasma reactor.

Table 1
Processing conditions of the ZnO nano-powder

Specimen name	R-ZnO	T-ZnO	S-ZnO
Plasma-forming gas	50% Ar 50% N_2	50% Ar 50% N_2	100% N_2
Carrier gas	Air	N_2	N_2
Quenching gas	Air	Air + N_2	Air + N_2

ing nitrogen into ZnO nanoparticles was achieved by introducing nitrogen gas into the plasma-forming and carrier gases. Flow rates of the plasma, carrier and quenching gases are respectively in the range of 200, 10 and 3000 slm. The processing conditions are summarized in Table 1. Chemical compositions of the resulting nanoparticles are listed in Table 2.

2.2. Characterization of ZnO nanoparticles

The phase identity and crystallite size of the ZnO nanoparticles were determined using an X-ray diffractometer (XRD, Philip PW1700) operated at 40 keV and 40 mA with Cu Kα radiation. The scanning step size and the collection time for each step were set at 0.02° and 5 s, respectively. Nanocrystal size was analyzed through broadening of the XRD peaks

Table 2
Specific surface area (BET) and chemical analysis of the ZnO nanoparticles

Specimen	BET ($m^2\ g^{-1}$)	Pb (ppm)	Cr (ppm)	Fe (ppm)	N (ppm)
R-ZnO	7.2	10	<1	1.8	1250
T-ZnO	7.5	41.0	<1	1.8	1200
S-ZnO	15.1	30.0	<1	1.8	1770

using the Scherrer's formula as follows:

$$B_s = \frac{0.94\lambda}{d\cos\theta} \quad (1)$$

where B_s is the broadening from the sample, λ the wave length of X-ray, d the crystal size, θ the Bragg's angle. In addition, instrumental broadening (B_I) caused by slit width, sample size, sample penetration, imperfect focusing, and non-monochromaticity of the beam (α_1 and α_2 for example) was carefully calibrated. Assuming Gaussian shape for the peaks, the broadening from the sample (B_s) is calculated through

$$B_s^2 = B_m^2 - B_I^2 \quad (2)$$

where B_m is the measured broadening.

A field emission scanning electron microscope (FE-SEM, LEO 1530) and a transmission electron microscope (TEM, Jeol 2010) were used for morphological observations of the ZnO nanoparticles. The specific surface area of the resultant ZnO powders was determined by a nitrogen gas adsorption instrument (Micrometrics ASAP 2010) based on the BET method. Nitrogen elemental analysis was done with a nitrogen/oxygen determination (LECO Corporation, TC-436). The chemical composition of the nanoparticles was analyzed by an inductively coupled plasma-mass spectrometer (ICP-MS, Spectro-P).

2.3. Photocatalytic testing

Methylene blue (MB) decomposition and anti-microbial testings were carried out to study photocatalytic ability of the ZnO nanoparticles. Based on the Beer–Lambert law [24], the methylene blue aqueous solution with 10^{-5} M is linearly proportional to the intensity of the measured spectrum. In the present study, the MB (10^{-5} M) solutions containing 0.2 wt.% of well-dispersed ZnO nanoparticles were illuminated employing a 6 W Xenon UV-lamp with the wavelength of 365 nm and a 13 W fluorescent lamp. To ensure no UV light radiation, irradiation from the fluorescent lamp was filtered through a 400 nm UV cut filter. The incident intensities of illumination of the UV and the visible light were set to 750 μW cm^{-2}, and 7000 lx, respectively. Photocatalytic decomposition of the MB solutions was characterized by a UV–vis spectrometer (HITACHI U-3010). The wavelengths that are prevailingly absorbed by MB are 665, 292, and 246 nm whereas the maximum peak occurs at 665 nm. The extent of decomposition was calculated from the integrated area of the peak at 665 nm.

Anti-microbial experiments using *Escherichia coli* (BCRC 11634) were performed with the suspension containing 0.2 wt.% ZnO nanoparticles of specimen in distilled water. The same bacteria were also cultured in distilled water as a reference specimen. Both samples were illuminated with the wavelength of 543 nm UV light and the intensity of 1500 lx for 6 h. Afterward, the samples were examined in the number of bacterium using an optical microscope.

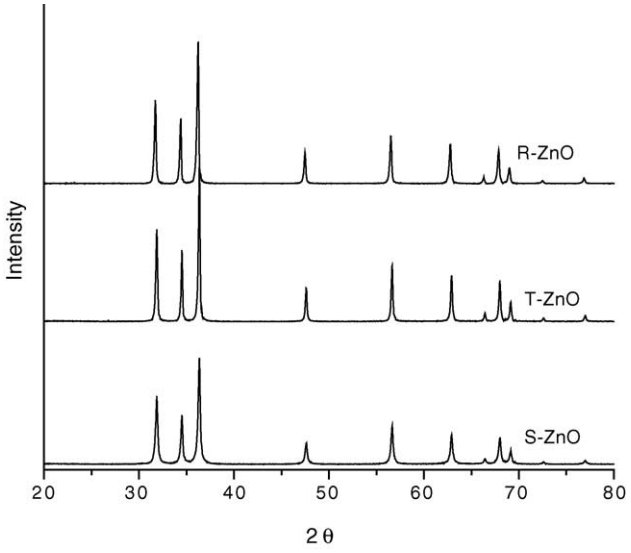

Fig. 2. XRD patterns of the ZnO nanoparticles.

3. Results and discussion

The crystalline structure of all the synthesized ZnO nanoparticles in the present study is hexagonal wurtzite structure (space group $P6_3mc$). Fig. 2 is the XRD profiles of the nanoparticles. It has been reported [25] that ZnO particles formed by oxidation of Zn vapor typically show two kinds of shapes: granular and tetrapod-like. In the present study, various morphologies of ZnO nanoparticles, namely, rod-like (R-ZnO), tetrapod-like (T-ZnO), and spherical (S-ZnO), have been synthesized as shown in Fig. 3. Average particle size of the spherical ZnO calculating from the broadening of the XRD peaks is about 31 nm. The tetrapod-like particles consist of four crystalline rods with a diameter and a length of about 30 and 100–200 nm, respectively, as shown in Fig. 3(d). It appears that the kind of plasma affects the nanoparticle morphology and N_2 plasma favors formation of the spherical nanoparticles. As listed in Table 2, specific surface areas (BET) of the nanoparticles varied from 7.2 to 15.1 g cm^{-3}, which indicates a certain extent of agglomeration in the powders.

Typical TEMs of the spherical and tetrapod-like ZnO nanoparticles are shown in Fig. 4. It is seen from Fig. 4(a) of the tetrapod-like particles that shape of the crystalline needle perpendicular to the micrograph (i.e. parallel to the e-beam) is hexagonal in the cross section. Since the e-beam is in the [0 0 0 1] direction and thus the ZnO needle grew in the ⟨0 0 1⟩ direction [25]. As showed in Fig. 4(b) of the spherical nanoparticles, the distance between lattice planes is measured to be 5.2 Å corresponding to the lattice constant C_0 of wurtzite ZnO.

Fig. 5 shows the typical diffuse reflection spectra of the nitrogen-doped ZnO nanoparticles and commercial ZnO powders (Japan High Purity Chemicals) for comparison. Note that in the present study, nitrogen-doping concentration in the nanopowders is typically in the range of about 1200–1800 ppm. We observed a strong absorption edge below 420 nm and a significant absorption in the visible range

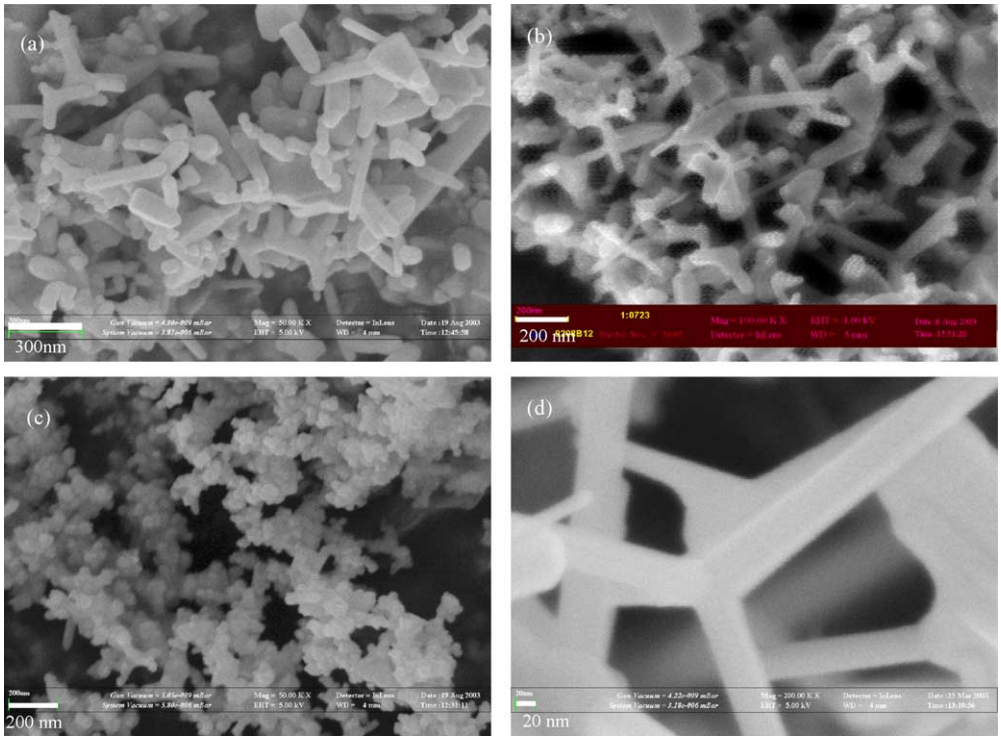

Fig. 3. FESEM images of (a) R-ZnO, (b) T-ZnO, (c) S-ZnO, and (d) a close-up of the T-ZnO nanoparticles.

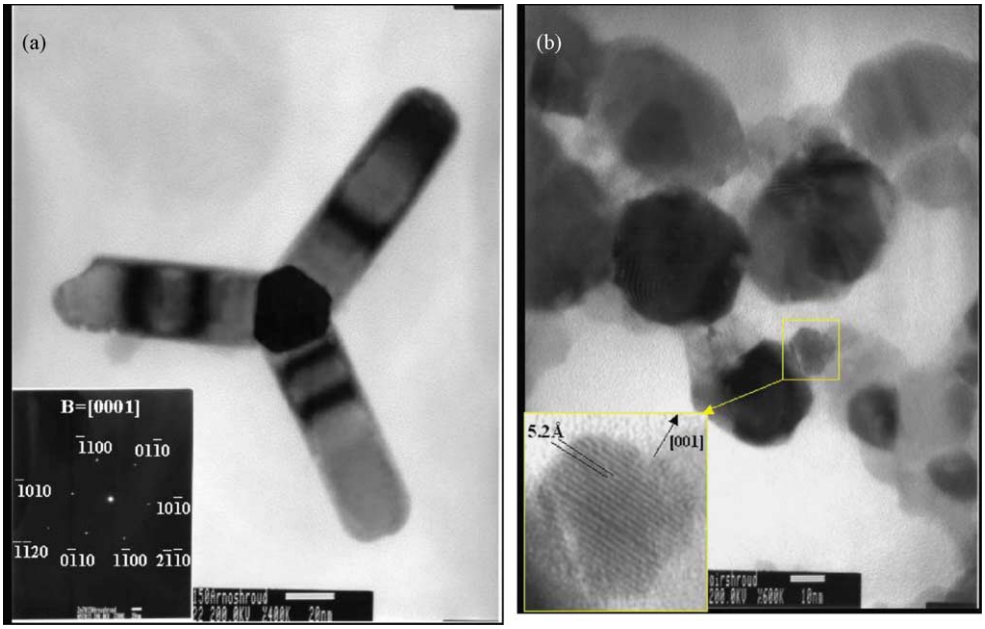

Fig. 4. Transmission electron micrographs of (a) tetrapod-shaped and (b) spherical ZnO nanoparticles.

from 450 to 650 nm. And it appears that in the visible range there exists an absorption edge at about 500 nm, corresponding to a band gap of 2.5 eV. The visible range absorption may be ascribed to a defect of energy state induced by nitrogen in the ZnO band gap. Since doping N (column V) in substitution for O (column VI) in ZnO forms the p-typed semiconductor [26], the defect level or acceptor level is near the valence band.

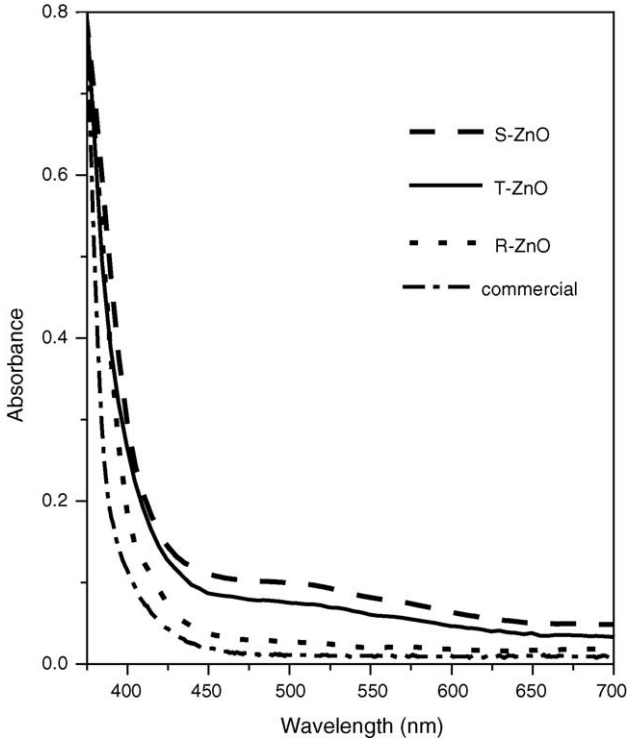

Fig. 5. UV–vis absorption spectra of the ZnO nanoparticles.

Li and Haneda [20] reported two absorption edges at about 385 and 500 nm for the nitrogen-doped ZnO particles synthesized by spray pyrolysis of zinc-ammonia solution. Futsuhara et al. [27] reported that the optical band gap of ZnO films decreased from 3.26 to 2.3 eV when the nitrogen concentration increased from 0 to 10 at.%. The decrease in band gap was attributed to a decrease in ionicity due to the formation of Zn–N bands.

It is worthwhile to mention that Irie et al. [23] recently reported that increasing the nitrogen concentration in $TiO_{2-x}N_x$ lowered the quantum yields when irradiating with UV light, indicating that the doping sites could also serve as recombination sites. Li and Haneda [20] reported that the visible photocatalysis of ZnO powder was significantly improved by doping a small amount of nitrogen. However, there exists an optimal amount of doping concentration due to excess N-dopant resulting in instability of the material.

It is known that conduction band electrons (e^-) and valence band holes (h^+) are generated on the surface of ZnO particles when aqueous ZnO suspension is illuminated by light with energy greater than the band gap energy, as demonstrated in R1. Holes can react with water adhering to the surface of ZnO nanoparicles to form highly reactive hydroxyl radicals ($OH^\bullet$), as shown in R2. Oxygen acts as an electron acceptor by forming a super-oxide radical anion ($O_2^{\bullet -}$), as shown in R3. The suspension of super-oxide radical anions may act as oxidizing agents or as an additional source of hydroxyl radicals via the subsequent formation of hydrogen peroxide as shown in R4–R6. The powerful oxidants associated with hydroxyl radicals react with the Methylene blue (MB^+), and make the blue solution colorless, as shown in R7. Since decomposition reaction of the MB is composed of several steps,

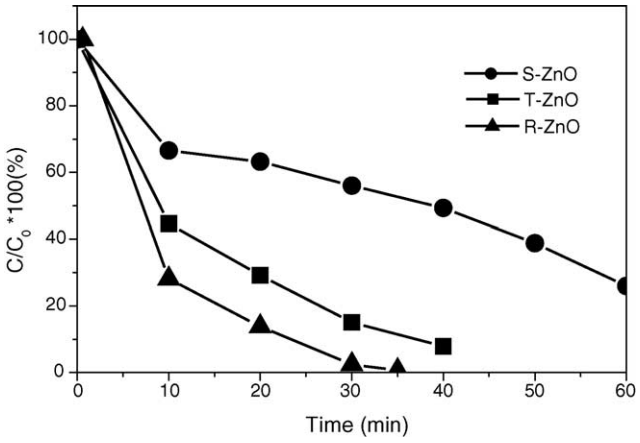

Fig. 6. Degradation of the MB under UV irradiation as a function of time for the various ZnO nanoparticles.

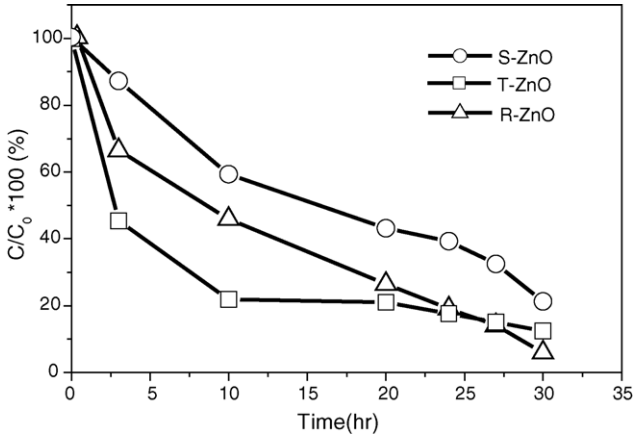

Fig. 7. Degradation of the MB under visible light irradiation as a function of time for the various ZnO nanoparticles.

R7 is just a simplified form

$$ZnO + h\nu \rightarrow e^- + h^+ \quad (R1)$$

$$H_2O + h^+ \rightarrow OH^\bullet + H^+ \quad (R2)$$

$$O_2 + e^- \rightarrow O_2^{\bullet -} \quad (R3)$$

$$O_2^{\bullet -} + H^+ \rightarrow HO_2^\bullet \quad (R4)$$

$$2HO_2^\bullet \rightarrow H_2O_2 + O_2 \quad (R5)$$

$$H_2O_2 + O_2^{\bullet -} \rightarrow OH^\bullet + O_2 + OH^- \quad (R6)$$

$$OH^\bullet + MB^+ \rightarrow \text{colorless compound} \quad (R7)$$

Fig. 6 shows degradation of the MB solution under the UV irradiation ($\lambda = 365$ nm) as a function of time for various ZnO nanoparticles. It is seen that the decomposition rates for all samples are high within the first 10 min. As MB concentration decreases, probability of MB molecules reacting with ZnO nanoparticles decreases and consequently decomposition rate decreases. The overall decomposition rates associated with individual specimens decrease in the order: R-ZnO > T-ZnO > S-ZnO. Note that even though possessing the highest specific surface area, the S-ZnO sample has the lowest MB decomposition rate. It appears that particle morphology of the ZnO affect photocatalytic ability.

Degradation of the MB solutions under the visible light irradiation as a function of time for various ZnO nanoparticles is illustrated in Fig. 7. Similarly, the S-ZnO has the lowest decomposition rate among all specimens. It took 10 and 30 h, respectively, for specimens T-ZnO, and R-ZnO to decompose 80% of the MB solution. We note that photocatalytic ability of the ZnO nanoparticles may be additionally affected by the morphology and surface state of particles, dispersity in solution, and perhaps impurities in the sample.

Anti-bacterial mechanism of photocatalyze is as follows [28–32]. Under illumination, the powdered photocatalyst produces super-oxide ions and hydroxyl radicals that are very powerful oxidants. These highly reactive particles are able to oxidize organic materials and are effective against bacteria. When the cell membrane of bacteria is in contact with the powerful oxidants, it will be decomposed and consequently the bacteria will die. Photocatalyst not only kill the bacteria, but also clean their bodies. The body of a bacterium will be decomposed into carbon dioxide and water.

The anti-bacterial activity (A_b) is expressed as follows [33]:

$$A_b = \log_{10}\left(\frac{C_{re}}{C_s}\right) \quad (3)$$

where C_{re} is the germ count of reference (DI water) after irradiation; C_s the germ count of the sample. According to the Japan Industrial Standards (JIS 2801:2000), a sample is possessed of anti-bacterial function if the anti-bacterial activity is greater than 2 after 24 h since the reaction has started. Table 3 summarizes results of the anti-microbial test performed with the T-ZnO, the S-ZnO and a reference sample. Note that in the present study illumination duration for all samples is only 6 h. The anti-bacterial activity of the T-ZnO is calculated to be 2.25 whereas the S-ZnO to be 4.4. Contrary to results of the MB decomposition tests, the S-ZnO had better anti-microbial ability. The reason is not clear. Nevertheless, in view of the value of anti-bacterial activity, not only the S-ZnO but also the T-ZnO samples are effective anti-bacterial materials.

Table 3
The anti-bacteria tests performed with the ZnO

Sample name	Number of bacterium (CFU ml^{-1})		A_b
	C_s	C_{re}	
T-ZnO	4.7×10^2	8.4×10^4	2.3
S-ZnO	< 10	2.7×10^5	4.4

CFU: colony forming unit.

4. Conclusions

In this research, a novel dc thermal plasma reactor was used to produce ZnO photocatalyst nanoparticles with various morphologies. Visible light absorption of the ZnO photocatalyst was achieved by doping up to a few thousands ppm of nitrogen into the material. We found that under illumination of both UV and visible light, the spherical ZnO nanoparticles had better anti-microbial ability, while particles with tetrapod-like and rod-like shape had better MB decomposition ability.

Acknowledgment

The present work was supported by the Ministry of Economic Affairs in Taiwan under Contact No. 93-EC-17-A99-R6-0450.

References

[1] T. Sehili, P. Boule, J. Lemaire, J. Photochem. Photobiol. A 50 (1989) 103.
[2] J. Villasenor, P. Reyes, G. Pecchi, J. Chem. Technol. Biotechnol. 72 (1998) 105.
[3] M.D. Driessen, T.M. Miller, V.H. Grassian, J. Mol. Catal. A 131 (1998) 149.
[4] K.J. Klabunde, Nanoscale Materials in Chemistry, John Wiley and Sons, New York, 2001, 88 pp.
[5] H.K. Park, D.K. Kim, C.H. Kim, J. Am. Ceram. Soc. 80 (1997) 743.
[6] S.I. Hirano, Ceram. Bull. 66 (1987) 1342.
[7] D. Vorkapic, T. Matsoukas, J. Am. Ceram. Soc. 81 (1998) 2815.
[8] Y.X. Li, K.J. Klabunde, Chem. Mater. 4 (1992) 611.
[9] V.R. Palkar, Nanostruct. Mater. 11 (1999) 369.
[10] C.G. Granqvist, R.A. Burhman, J. Appl. Phys. 47 (1976) 2200.
[11] T.T. Kodas, Adv. Mater. 6 (1989) 180.
[12] G.L. Messing, S.C. Zhang, G.V. Jayanthi, J. Am. Ceram. Soc. 76 (1993) 2707.
[13] J.P. Pollinger, G.L. Messing, J. Aerosol Sci. Technol. 19 (1993) 217.
[14] G.D. Ulrich, J.W. Riehl, J. Colloid Interf. Sci. 87 (1982) 257.
[15] G. Skanadan, Y.J. Chen, N. Glumac, B.H. Kear, Nanostruct. Mater. 11 (1999) 149.
[16] A.K. Ghosh, H.P. Maruska, J. Electrochem. Soc. 124 (1977) 1516.
[17] Y. Masumoto, J. Solid State Chem. 126 (1996) 227.
[18] M. Anpo, Catal. Surv. Jpn. 1 (1997) 169.
[19] J. Araña, O. González Díaz, J.M. Doña Rodríguez, J.A. Herrera Melián, C. Garriga i Cabo, J. Pérez Peña, M. Carmen Hidalgo, J.A. Navío-Santos, J. Mol. Catal. A 197 (2003) 157.
[20] D. Li, H. Haneda, J. Photochem. Photobiol. A 155 (2003) 171.
[21] R. Asahi, T. Morikawa, T. Ohwaki, K. Aoki, Y. Taga, Science 296 (2001) 269.
[22] M. Jansen, H.P. Letschert, Nature 404 (2000) 980.
[23] H. Irie, Y. Watanabe, K. Hashimoto, J. Phys. Chem. B 107 (2003) 5483.
[24] H. Yoneyama, Y. Toyoguchi, H. Tamura, J. Phys. Chem. 76 (1972) 3460.
[25] Y. Suyama, Y. Tomokiyo, T. Manabe, E. Tanaka, J. Am. Ceram. Soc. 71 (1988) 391.
[26] M. Futsuhara, K. Yoshioka, O. Takai, Thin Solid Films 317 (1998) 322.
[27] D.P. Norton, Y.W. Heo, M.P. Ivill, K. Ip, S.J. Pearton, M.F. Chisholm, T. Steiner, Mater. Today 34 (2004).
[28] R. Asahi, T. Morikawa, T. Ohwaki, K. Aoki, Y. Taga, Science 293 (2001) 269.
[29] C.D. Jaeger, A.J. Bard, J. Phys. Chem. 83 (1979) 3146.
[30] J.R. Harbour, M.L. Hair, Adv. Colloid Interf. Sci. 24 (1986) 103.
[31] J.C. Ireland, J. Valinieks, Chemosphere 25 (1992) 383.
[32] R. Cai, K. Hashimoto, A. Fujishima, J. Electroanal. Chem. 326 (1992) 345.
[33] K.P. Kűhn, I.F. Chaberny, K. Massholder, M. Stickler, V.W. Benz, H.-G. Sonntag, L. Erdinger, Chemosphere 53 (2003) 71.